


Effect of Lead Addition and Milling on Densification and Mechanical Properties of 6061 Aluminium Alloys

Mahesh Paidpilli¹  · Kapil Verma¹ · Rajat Pandey¹ · Anish Upadhyaya¹

Received: 2 September 2016 / Accepted: 6 December 2016 / Published online: 23 December 2016
© The Indian Institute of Metals - IIM 2016

Abstract In the present work, one batch of prealloyed 6061Al powder was mixed with different lead compositions (5, 10, 15 vol.%) and another set with same composition was ball-milled for 5 h at 300 rpm. Microstructural features such as lattice constant, crystallite size, particle size and morphology were studied using XRD, particle size analyzer and SEM. Both the as-mixed as well as ball-milled powders were compacted at 300 MPa and sintered under N₂ atmosphere for 1 h in tube furnace at 590 °C. The ball milling of 6061Al alloy powder improved sinter density and densification while lead addition showed negligible influence on these parameters. The microstructure of as-mixed 6061Al–Pb alloys exhibited equiaxial morphology whereas ball-milling resulted in elongated grains with uniform lead distribution. Quasi-static compressive mechanical behavior was investigated for 6061Al–Pb alloys at $1 \times 10^{-3} \text{ s}^{-1}$ strain rate. Results indicated that ultimate compressive and yield strength were sensitive to milling and lead volume fraction.

Keywords 6061Al–Pb alloys · Mechanical alloying · Densification · Microstructure · Compression and sintering

1 Introduction

In the last few decades, aluminium based alloys have shown substantial interest in utilization by automobile industries due to their high strength to weight ratio [1].

These alloys possess excellent mechanical and physical properties such as specific strength, electrical conductivity, thermal conductivity, corrosion and wear resistance [2]. Al–Pb alloys are commonly used in automotive industries as a bearing material. Since, Pb is soft and a good thermal conductor, it acts as a lubricant between the wear surfaces [3–5].

Fabrication of Al–Pb alloy through conventional casting route arises difficulties. According to Al–Pb phase diagram [6] there is no mutual solubility in solid state and a large miscibility gap exists at higher temperatures. The massive difference in density and miscibility gap between aluminium and lead facilitate segregation of Pb during solidification [3–5]. Therefore, other methods have been developed such as powder metallurgy [7], rapid solidification [8] and stir-casting [9] to achieve homogeneous microstructure. The powder metallurgy is a viable processing route, it offers the feasibility to tailor the composition and microstructure of Al–Pb alloys.

Benjamin [10] developed the oxide dispersion strengthened (ODS) alloys by mechanical alloying. Since then, different kinds of alloys have been produced with various compositions in a wide range of metal, oxide and ceramic systems by mechanical alloying [3, 11]. Both Ranga et al. [5] and Zhu et al. [12] have reported homogeneous microstructure of Al–Pb system with fine grain size, achieved by high energy ball milling. Conventional press and sinter approach is cost effective and near net shape products can be produced by powder metallurgy route [13, 14].

The difficulties that arise during compaction and sintering are that, the Al powder easily welds to the die and oxide layer present between particle surfaces acts as a barrier to diffusion, respectively [15]. The prior factor has been addressed by using lubricant [16, 17] and the later one, by adding 1%

✉ Mahesh Paidpilli
maheshpaidpill@gmail.com

¹ Department of Materials Science and Engineering, Indian Institute of Technology, Kanpur 208016, India

Mg to disrupt oxide layer by forming spinel [18]. An extensive work has been done and published on liquid phase sintering of aluminium alloys under N_2 atmosphere, and their report shows enhancement in densification, sinterability and mechanical properties [19, 20]. Several researcher have investigated the influence of trace elements such as lead, tin and antimony on sintering and tensile behavior of aluminum alloy [21–23]. However, few investigations have been conducted to examine the compressive behavior of Al–Pb system at room temperature [24].

A lot of work has been reported on the utilization of Al–Pb alloys in the manufacturing of bearing material by many researchers but none have worked on 6061Al–Pb system by conventional press and sinter route to the best of our knowledge. Therefore, in the present work, prealloyed 6061 powder mixed with elemental powder (Pb) has been compacted and sintered to study the sintering and mechanical behavior. Moreover, this investigation estimates the effect of mechanical alloying and lead volume percentage on densification, microstructural and mechanical properties of 6061Al–Pb alloys. An attempt has also been made to compare as-mixed and ball-milled 6061Al–Pb alloy consolidated by liquid phase sintering on the basis of particle size, strain, compressive strength and hardness.

2 Experimental Procedure

The pre-alloyed 6061Al powder was supplied by Cegedur Pechiney, Hermillon; France and lead powder by Sigma-Aldrich. As-received 6061Al powder was mixed with varying amounts of lead (5, 10, 15 vol.%) using turbula mixer. In another set of experiment, same composition of constituent powder were co-milled. Zhu et al. [12] and Sheng et al. [25] documented that milling Al–Pb alloys beyond 5 h had very little variation in parameters such as lattice constant and grain size. In addition, Suryanarayana [11] also reported that pre-alloyed powder required less milling time as compared to elemental powder to achieve the same effect. Hence, ball milling was performed for 5 h in wet condition using planetary ball mill (FRITSCH, Pulverisatte, Germany) at 300 rpm with ball to powder ratio of 10:1. The morphology of the powders were observed under scanning electron microscope (QUANTA 200, FEI, The Netherlands). The differential scanning calorimetry (DSC) and thermogravimetric analysis (TGA) were conducted on prealloyed 6061Al powder using STA 8000 (PerkinElmer) under N_2 atmosphere. The heating and cooling rate was $10\text{ }^\circ\text{C}/\text{min}$. The particle size of powders were measured by particle size analyzer (Malvern mastersizer 2000). The phases present in the powder and sintered specimen were characterized using X-Ray diffractometer (Bruker AXS Diffraktometer D8, Germany) with Cu-K_α ($\lambda = 1.54060\text{ \AA}$)

as the incident wavelength. The scanning range was kept $20^\circ\text{--}90^\circ$ at a scanning rate of 1° per min in step size of 0.02° . The Williamson–Hall method [26] was used to calculate the crystallite size and lattice strain of the powders. The processed powders were compacted at 300 MPa load to obtain cylindrical pellets (16 mm diameter, 7 mm height) in a uniaxial semi-automatic hydraulic press (CTM-50; Ichalkaranji, India). Zinc stearate was applied on die wall before each run for lubrication purpose. The green compacts were sintered under N_2 in a tube furnace (OKAY 70T-7, Bysakh, Kolkata, India) at a sintering temperature of $590\text{ }^\circ\text{C}$. The holding time was 1 h with a heating rate of $5\text{ }^\circ\text{C}/\text{s}$. Geometric dimension and weight was measured to determine the green density of compacts with an accuracy of $\pm 0.001\text{ mm}$ and $\pm 0.001\text{ g}$. The sinter density of sintered compact was calculated by Archimedes principle using a microbalance (AG245, Mettler Toledo, Switzerland) and distilled water (density $\sim 0.99681\text{ g}/\text{cm}^3$) was used as an immersion medium. In all the above measurements, averaged value of three samples was reported. Densification parameter was calculated using Eq. (1)

$$\text{Densification parameter} = \frac{\text{Sinter density} - \text{Green density}}{\text{Theoretical density} - \text{Green density}} \quad (1)$$

where, the theoretical density of the sample was calculated using inverse rule of mixing. Sintered samples were prepared for standard metallographic examination by grinding on emery paper of grit sizes (320, 500, 1000, and 1600). Thereafter, the sample was polished with alumina suspension using a series 1, 0.3 and $0.05\text{ }\mu\text{m}$, followed by $0.04\text{ }\mu\text{m}$ colloidal silica in manual polisher (Lunn Major, Struers, Denmark). The microstructure was observed under scanning electron microscope (QUANTA 200, FEI, The Netherlands). Universal hardness tester (Tinius Olsen) was used to determine Vickers hardness of all sintered samples. The load applied was 5 kg with holding time of 10 s. An average of ten indentations were made on each sample and the results were reported. Compression tests were performed using universal testing machine (Instron-1195) at constant strain rate $1 \times 10^{-3}\text{ s}^{-1}$ as per ASTM E9-09. Cylindrical sample (height = 6 mm, diameter = 4 mm) were cut from sintered compacts using wire EDM (STX-202).

3 Results and Discussion

3.1 Powder Morphology

Figure 1 shows the SEM photomicrographs of prealloyed 6061Al and lead powders. Prealloyed 6061Al particles have spherical structure with particle size ranging between $14\text{--}70\text{ }\mu\text{m}$. Whereas, lead particles are irregular and round

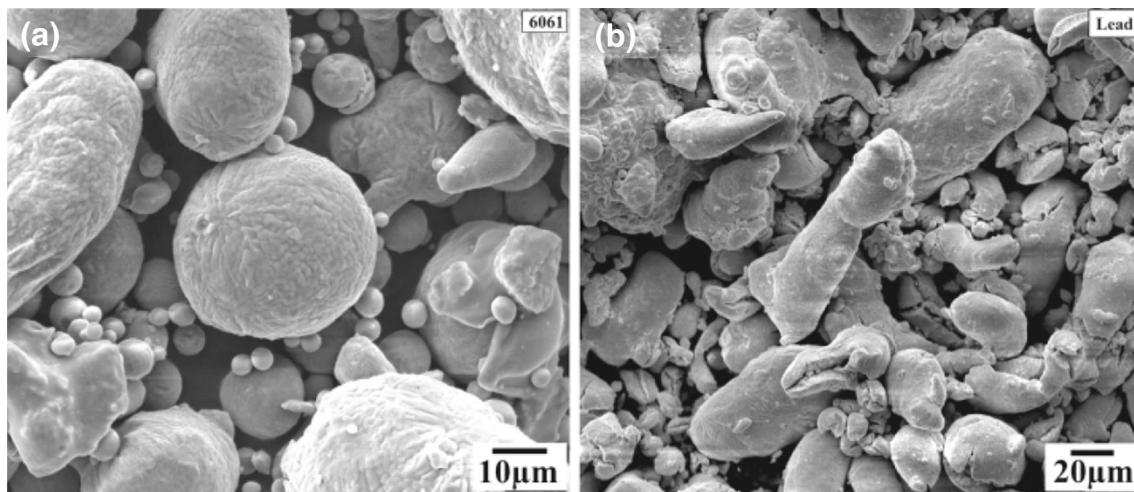


Fig. 1 Morphology of **a** 6061Al powder and **b** lead powder in as-received condition

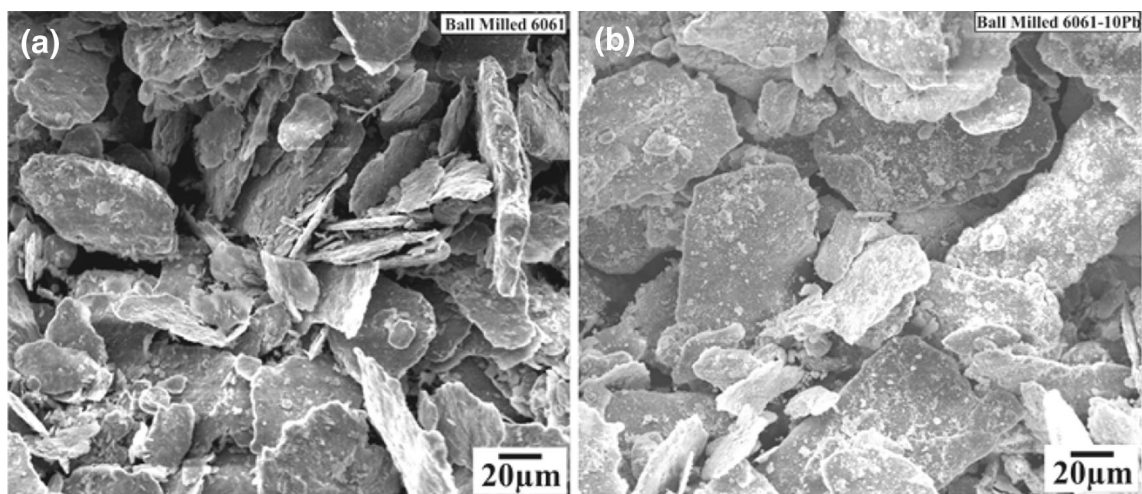


Fig. 2 Morphology of ball-milled **a** 6061Al powder and **b** 6061Al–Pb alloy powder

shaped with size range of 10–62 μm . Figure 2 shows the SEM photomicrographs after wet milling of investigated powders. The ball milled 6061Al have flake structure with particle size ranging between 14 and 90 μm while ball milled Al6061–10Pb have particle size between 20 and 105 μm . The morphology results indicate that during milling, addition of lead acts as a binder to increase the particle size by cold welding and reduces the fracturing of particles [11]. This has been confirmed using particle size analyzer and shown in Table 1 and Fig. 3.

3.2 Structural Analysis

The X-ray diffraction peaks of investigated powders include the instrumental effect. To remove this effect, instrumented–corrected broadening β_D [27] corresponding to the full width half maxima of diffraction peak of Al has

been determined using the Eq. (2). The instrumental broadening has been measured using XRD pattern of standard silicon material.

$$\beta_D^2 = \beta_{\text{measured}}^2 + \beta_{\text{instrumental}}^2 \quad (2)$$

The Williamson–Hall method [26] considers both crystallite size and microstrain through width broadening analysis. Scherrer equation [28] estimates the crystallite size using Eq. (3).

$$D = \frac{k\lambda}{\beta_D \cos \theta_{hkl}} \quad (3)$$

Strain induced due to distortion and crystal imperfections present in peak broadening are related by $\varepsilon \approx \beta_S / \tan \theta$ [29]. According to Williamson–Hall method:

$$\beta_{hkl} = \beta_D + \beta_S \quad (4)$$

Table 1 Effect of initial powder preparation condition (mixing versus milling) on the powder size of 6061Al and 6061Al–10Pb

Properties	6061Al alloy		6061Al–10Pb alloy	
	As-mixed	Ball-milled	As-mixed	Ball-milled
Particle size (μm)				
D ₁₀	14.2	14	13.4	20.4
D ₅₀	35.5	42	32.7	54
D ₉₀	70.5	90.9	66.9	105.8

$$\beta_{hkl} = \frac{k\lambda}{D \cos \theta_{hkl}} + 4\epsilon \tan \theta_{hkl} \quad (5)$$

Rearranging Eq. (5)

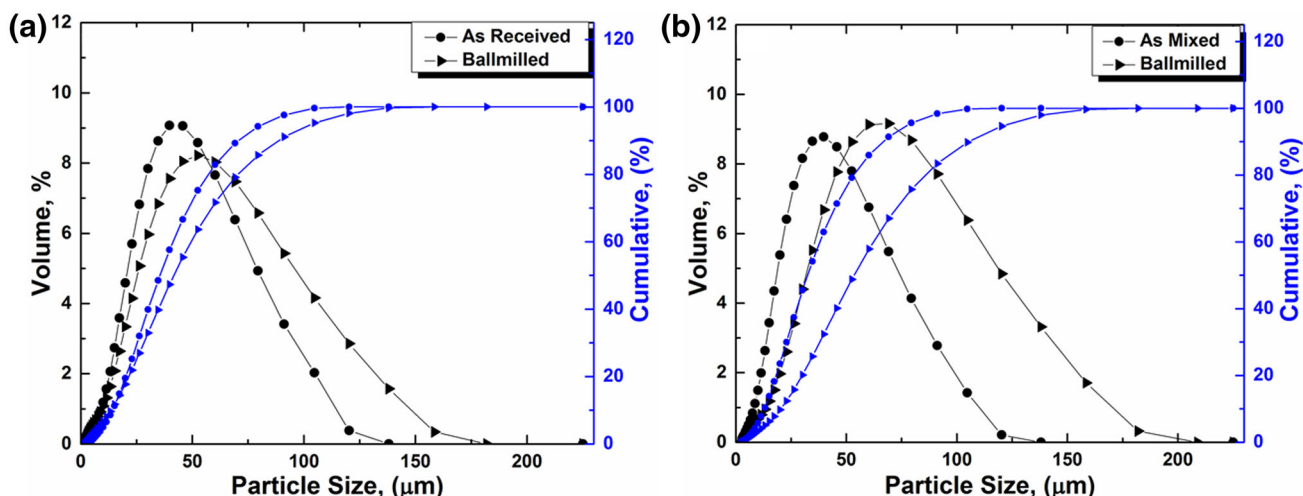
$$\beta_{hkl} \cdot \cos \theta_{hkl} = \frac{k\lambda}{D} + 4\epsilon \sin \theta_{hkl} \quad (6)$$

where, β_{hkl} is the corrected full width half maxima, θ_{hkl} is the Bragg angle, λ is the wavelength of X-rays and k is the shape factor (0.94). Figure 4a shows the XRD pattern of as-received 6061Al and ball-milled 6061Al with and without Pb addition. The full width half maxima of Al peak for (111), (200), (202) and (311) planes has been measured using MDI Jade software and instrumental broadening correction has been performed. These diffraction peaks attribute to FCC phase structure. Figure 4b shows the plot between $\beta \cos \theta$ and $\sin \theta$ with linear fitting of as-received 6061Al, ball-milled 6061Al and 6061Al–10Pb powders. The three peaks have been used to construct a straight line having maximum goodness of fit out of four Al peak (111), (200), (202) and (311). Crystallite size and strain of these powders have been measured from the intercept and slope of the linear fitted line, respectively. The effect of milling and lead addition on lattice constant, crystallite size and strain have been calculated for these powders using Eq. (1)

and shown in Table 2. The matrix crystallite size of Al6061 powder after milling for 5 h gets reduced to 70.2% while in case of Al6061–10Pb, it is reduced to 59.6%. After 5 h milling, more strain has been introduced in the powder due to plastic deformation caused by milling and addition of lead shows negligible effect on strain. During milling, some minor alloying elements related to process control agent or Al are dissolved by atomic diffusion and decreases the lattice parameter [30, 31] as shown in Table 2. Figure 5 shows the XRD pattern of sintered ball-milled and as-mixed 6061Al compact with varying amount of lead. The diffraction peak intensities of lead increases with increase in lead volume fraction. It has been observed that after milling, the diffraction peaks broadens and shifts to right due to structural refinement. It has also been observed that milled powder have more relative Pb peaks as compared to as-mixed powder. The matter is not yet resolved and is stated as such. However, one reason can be that during sintering, the heavy Pb melt formed in as-mixed 6061Al–Pb alloy may sink below the surface due to presence of gravity. While, in case of milled powder, the increased surface area of lead and Al–Pb bond restrain the above sinkage.

3.3 Thermal Analysis of As-Received 6061Al Powder

Figure 6a shows the DSC curve of as-received 6061Al powder during heating and cooling cycle. The endothermic peak indicates the melting of as-received 6061Al powder at 651.49 °C and 581 °C is the onset temperature of liquid formation. Hence, sintering temperature has been chosen as 590 °C to obtain sufficient densification through rearrangement and grain shape accommodation [32]. Figure 6b shows the TGA curve of as-received 6061Al powder during heating under N₂. It has been observed that till 430 °C

**Fig. 3** Particle Size distribution of as-received and ball-milled **a** 6061Al and **b** 6061Al–10Pb alloy powders

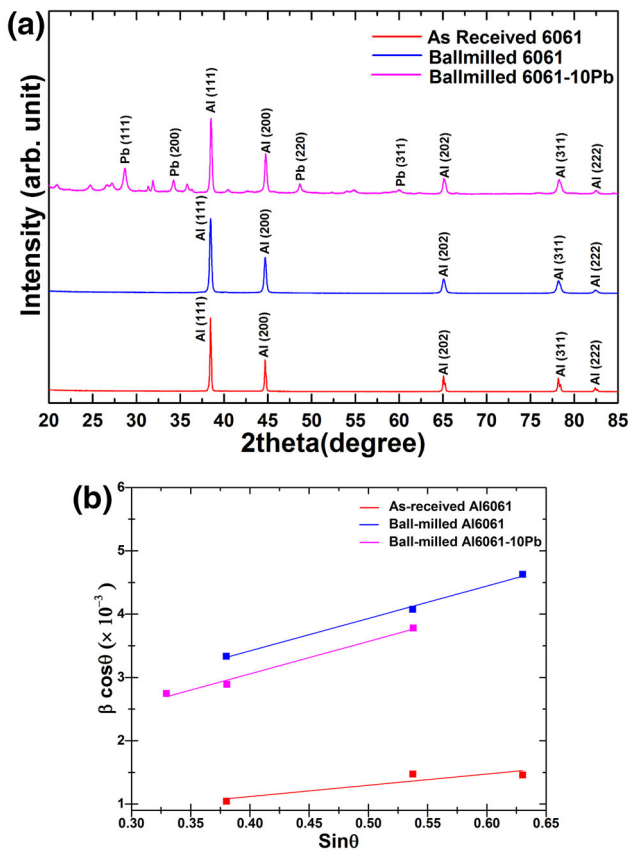


Fig. 4 a XRD patterns and b W–H analysis of 6061Al alloy powder (as-received and ball-milled condition) and ball-milled 6061Al–10Pb powder

weight loss during heating due to removal of moisture and volatile matter. Thereafter it’s stabilized and at around 545 °C the weight starts increasing due to formation of aluminium nitrate structure [33, 34].

3.4 Densification Behavior of Sintered Compacts

The effect of lead on green density of 6061Al powders compacted at 300 MPa pressure are shown in Fig. 7a. This curve indicates that compressibility of ball-milled 6061Al powder is lower than as-mixed 6061Al powder. Since, strain was introduced in the powder during milling, which causes decrease in compressibility [35]. The increase in volume fraction of lead has little influence on

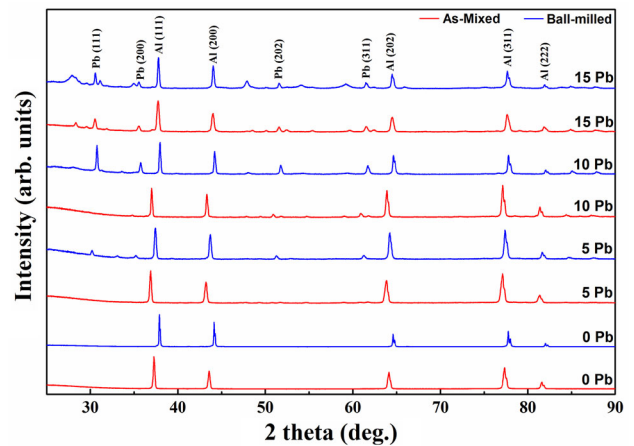


Fig. 5 Effect of Pb addition and powder processing condition (as-mixed and ball-milled) on the phase formation in 6061Al alloys sintered at 590 °C

compressibility due to higher density of lead as compared to 6061Al alloy. Figure 7b shows the effect of milling on sintered density as a function of lead content. The results show that in all the cases, density increases after sintering except pure 6061Al alloy due to swelling of specimen. However, with lead addition, density increases in case of as-mixed 6061Al alloy but increase in lead volume fraction shows negligible effect. This behavior attributes to little amount of liquid produced in 6061Al alloy at 590 °C as shown in Fig. 6. In contrast, lead addition produces liquid which provides appreciable rearrangement and densification during sintering [36]. In case of ball-milled 6061Al alloy, sinterability is higher as compare to as-mixed 6061Al alloy. Strain and surface energy act as driving force for sintering [35]. On the other hand, addition of 5 vol. % Pb decreases the sintered density. Since, the particle size of ball-milled 6061Al-Pb powder is increased, which reduces the sinterability [35]. However, as lead volume fraction increases, the sinter density increases from 90.6 to 95.2% theoretical density. This behavior indicates large amount of liquid formation which, compensate for the increased particle size. Figure 7c graphically presents the effect of milling and lead content on 6061Al alloy sintered at 590 °C on densification parameter. The results show similar trend as in case of sintered density curve. As-received 6061Al alloy have negative densification parameter which

Table 2 The crystallite size and lattice strain of 6061Al alloy (in as-mixed and ball-milled condition) and ball-milled 6061Al–10Pb alloy powder

Powder	Lattice constant (Å)	Williamson–Hall method	
		Crystallite size (t) (nm)	Lattice strain (ε) (%)
As received 6061	4.053	355.2	0.045
Ball milled 6061	4.049	105.7	0.128
Ball milled 6061-10Pb	4.05	143.4	0.128

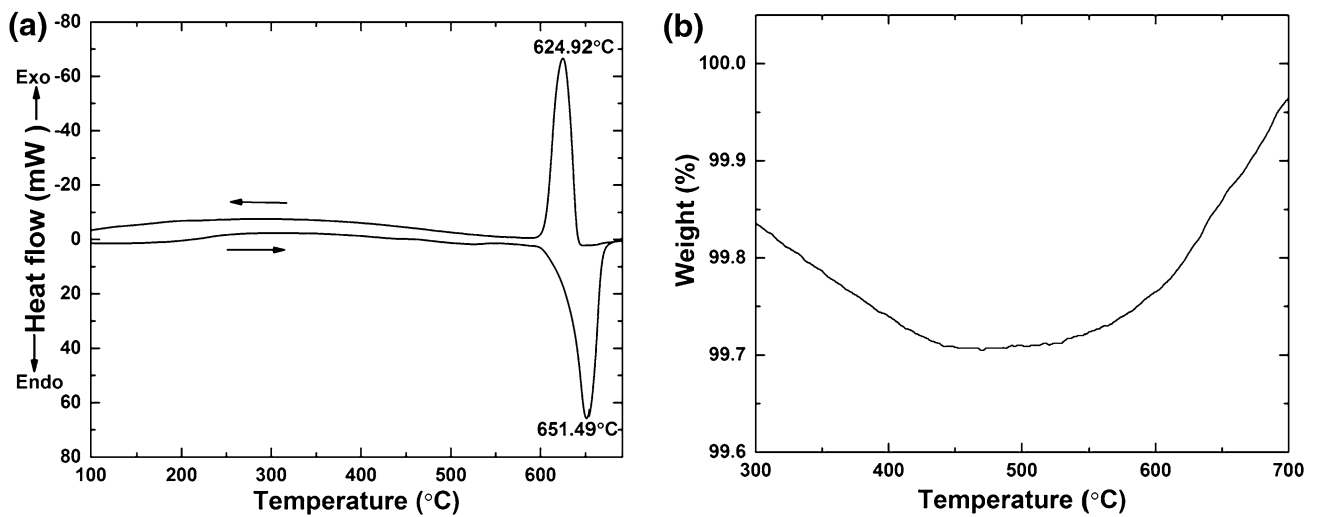


Fig. 6 a DSC and b TGA profile of as-received 6061Al alloy powder

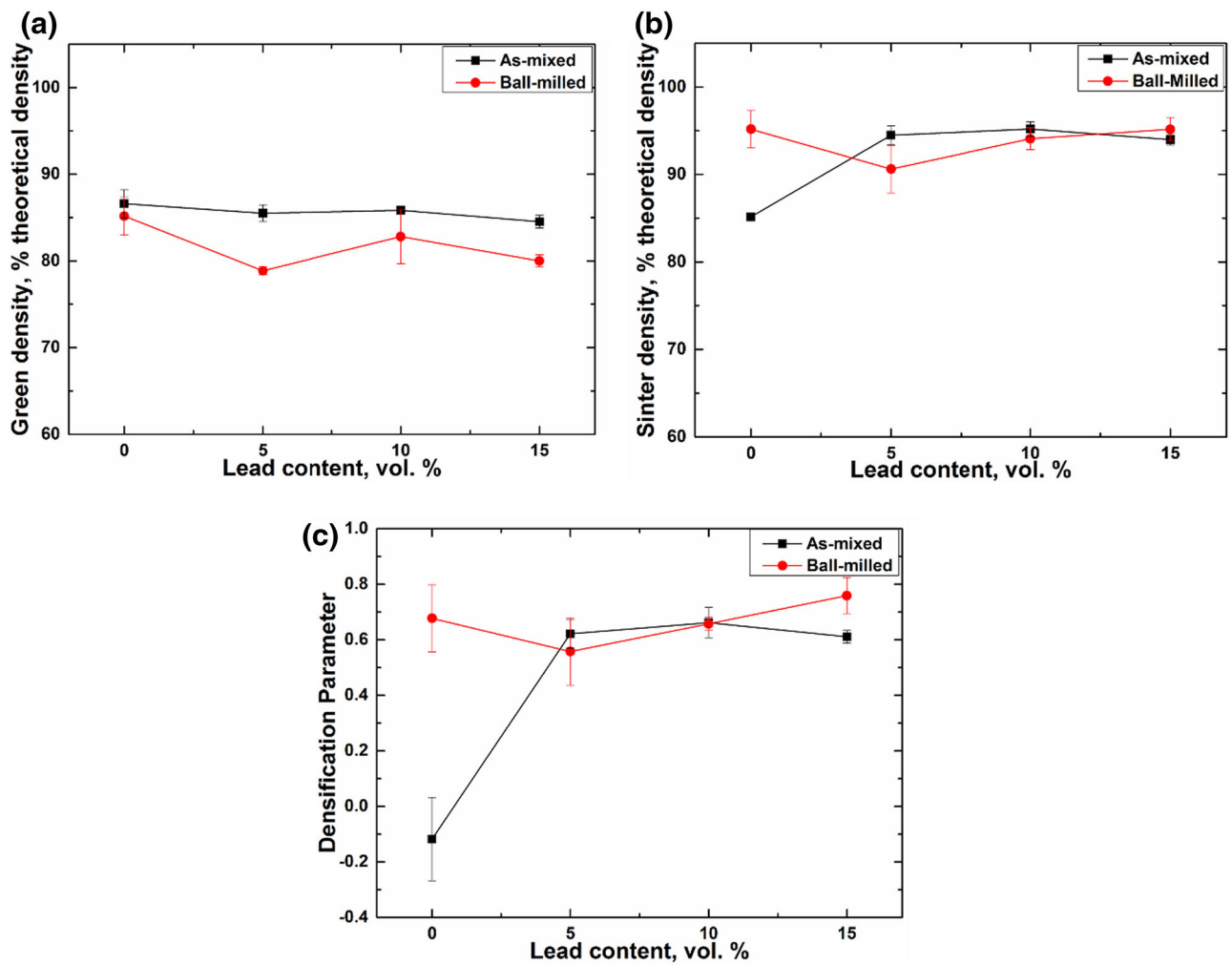


Fig. 7 Effect of lead content on a green density; b sintered density and c densification parameter of as-mixed and ball-milled 6061Al alloys

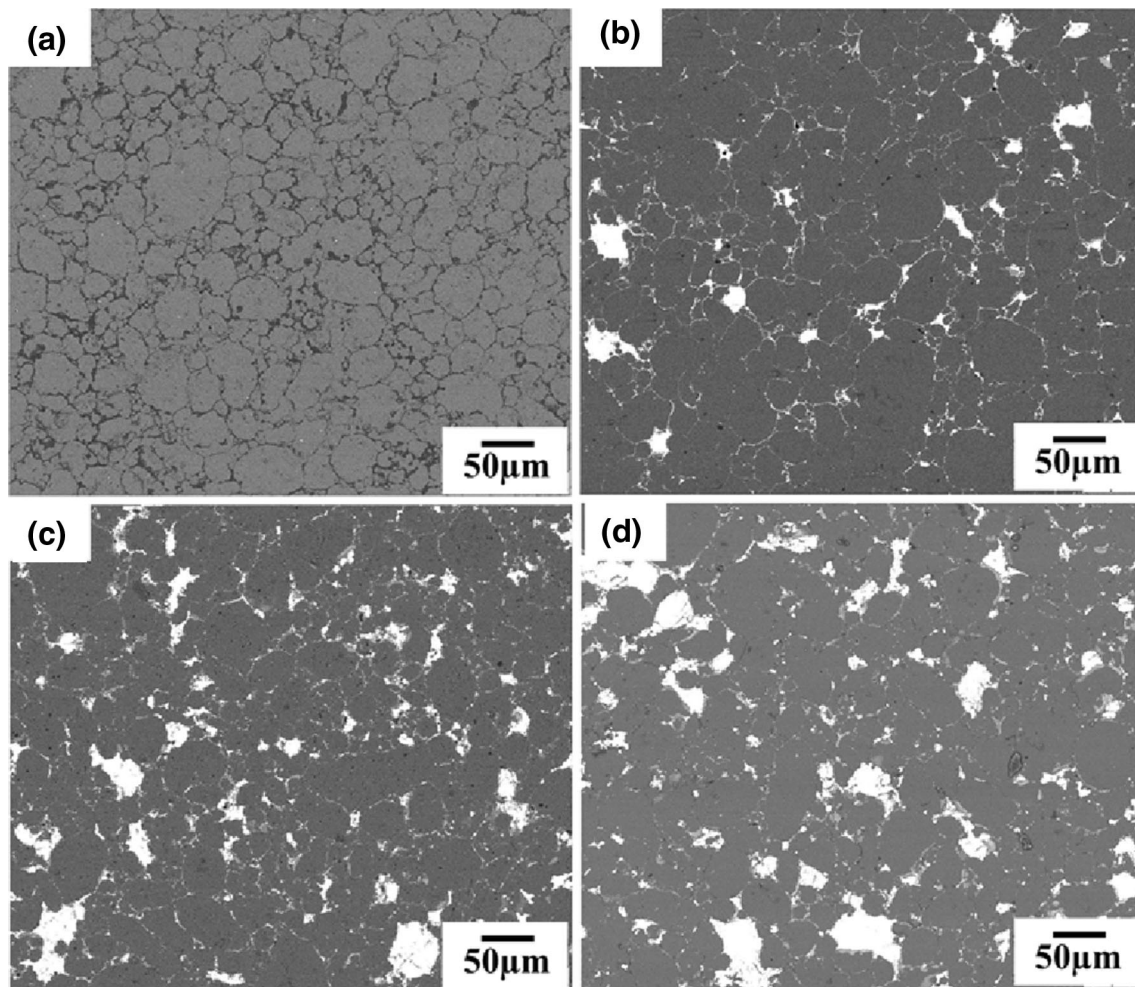


Fig. 8 SEM Photomicrographs of **a** 6061Al alloy and as-mixed 6061Al alloy with **b** 5%, **c** 10% and **d** 15 vol.% Pb, all compacts are pressed at 300 Mpa and sintered at 590 °C

represents swelling during sintering [14]. In general 6061Al alloy expands during sintering and this has also been reported by Gaur [37].

3.5 Microstructural Evolution

Figure 8a–d shows the effect of lead volume fraction on the representative microstructure of as-mixed 6061Al alloys. In Fig. 8a, the dark phase along the grain boundaries of Al has been analyzed using EDS and found rich in O, Mg and Si. During production of prealloyed 6061Al powder, supersaturated solid solution of Mg/Si is formed and hence on sintering it precipitates as Mg_2Si along the grain boundaries [38]. In initial stage of sintering, Mg reacts with Al_2O_3 to form spinel and hence disrupts the oxide layer. This happens due to diffusion of Mg through Al/ Al_2O_3 interface, which results in lattice expansion and induces shear stress along oxide layer [14, 18]. It is observed from Fig. 8b–d that Pb is non-homogeneously distributed and aluminum grains have equiaxial shape.

Since, lead is immiscible with base Al matrix, during sintering, lead segregates at liquid/vapor interface, which reduces the surface tension of melt [39]. Subsequently, it decreases the wetting angle, which enhances the spreading of melt along the grain boundaries. Figure 9a–d compares the effect of lead content on the microstructures of ball-milled 6061Al alloy sintered at 590 °C. The figure illustrates that milling for 5h and then sintering results in grain refinement as well as uniform distribution of lead. This attributes to better spreading of the melt in case of ball-milled compacts during sintering, which produces homogeneous distribution of Pb within the matrix.

3.6 Mechanical Properties

3.6.1 Bulk Hardness Measurement

Figure 10 compares the effects of lead content and milling on hardness of 6061Al alloys. The as-mixed sintered compact hardness increases with Pb content up to a

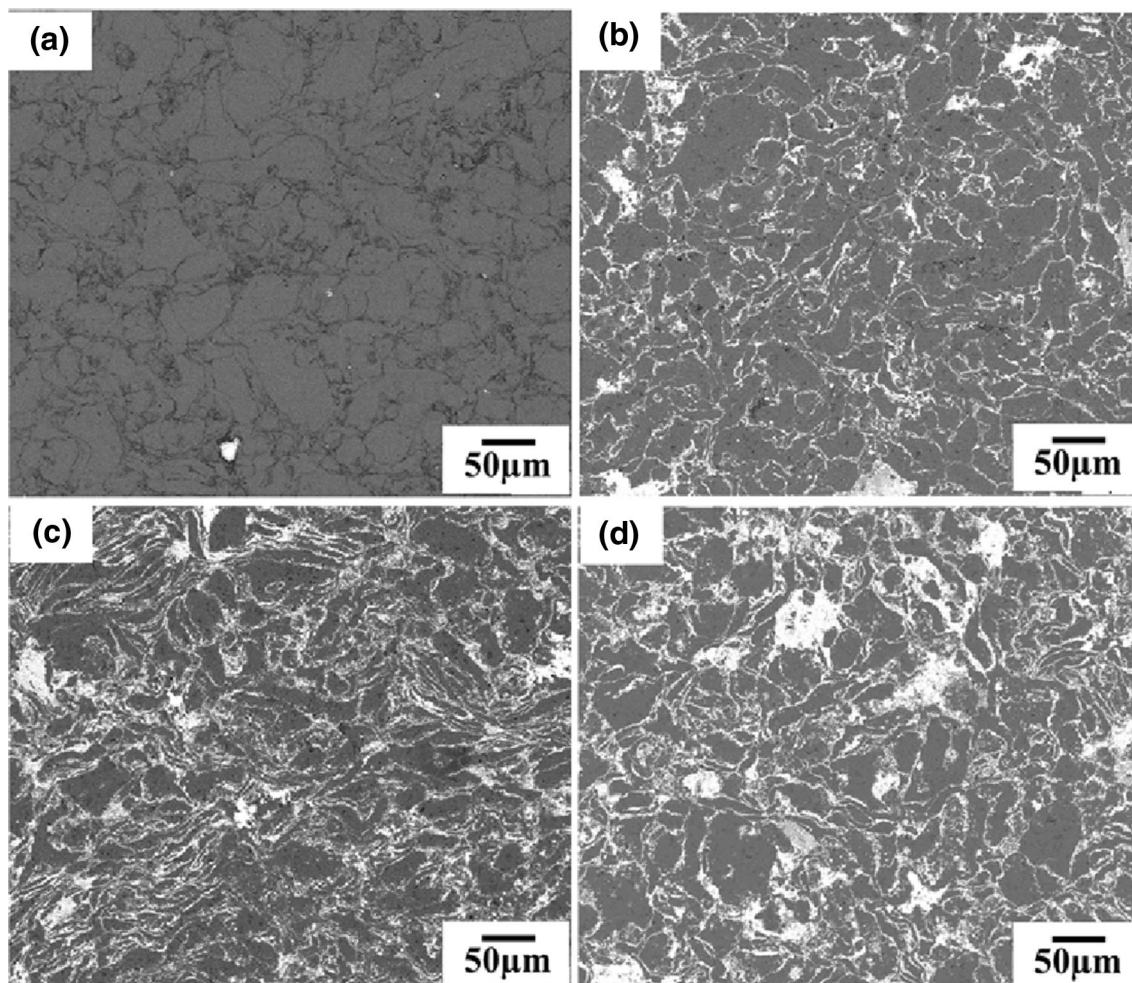


Fig. 9 SEM photomicrographs of ball-milled **a** 6061Al alloy and 6061Al–Pb with **b** 5%, **c** 10% and **d** 15 vol.%Pb in as-sintered condition

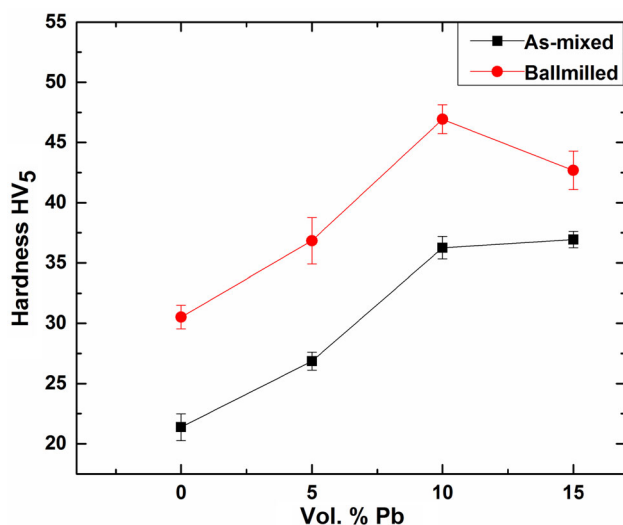


Fig. 10 Effect of lead addition and metal processing route on the bulk hardness of 6061 Al alloy compacts sintered at 590 °C

10 vol.%. The reason can be attributed to the presence of thin layer of Pb along the grain boundaries of Al matrix. Sheng et al. [25] have reported that gliding dislocation, shear the Pb particle and prevent the dislocation movement, which leads to improvement in hardness. However, with increase in Pb content, the accumulation of Pb as shown in Figs. 8 and 9 increases, which decreases the hardness value due to the soft nature of coarser Pb particle. It has been observed that all ball-milled sintered compacts show similar trend of variation, but have higher hardness value than their as-mixed counterparts. The reason for higher hardness value can be correlated to structural refinement, microstructure and uniform distribution of Pb along the grain boundaries of aluminum. The effect of addition of Pb on strengthening and softening of Al–Pb system depends on a number of variables such as, microstructure, grain size, deformation mechanism, volume fraction and distribution of lead [25, 38, 40].

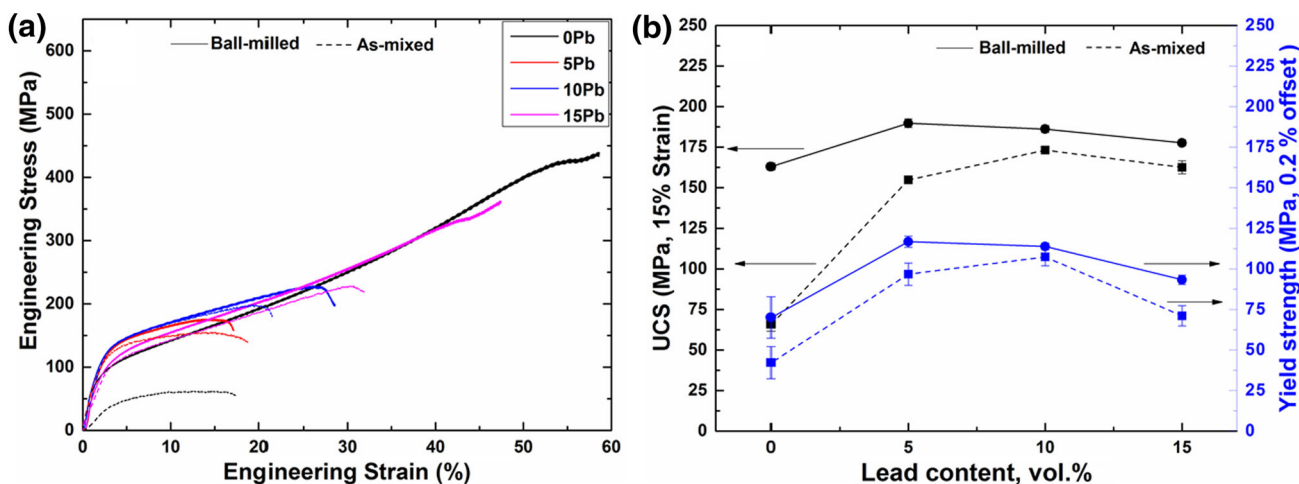


Fig. 11 Effect of lead content and processing condition (mixing and ball-milling) **a** engineering stress–strain and **b** strength (ultimate compressive strength and yield strength) of sintered 6061Al alloy compacts

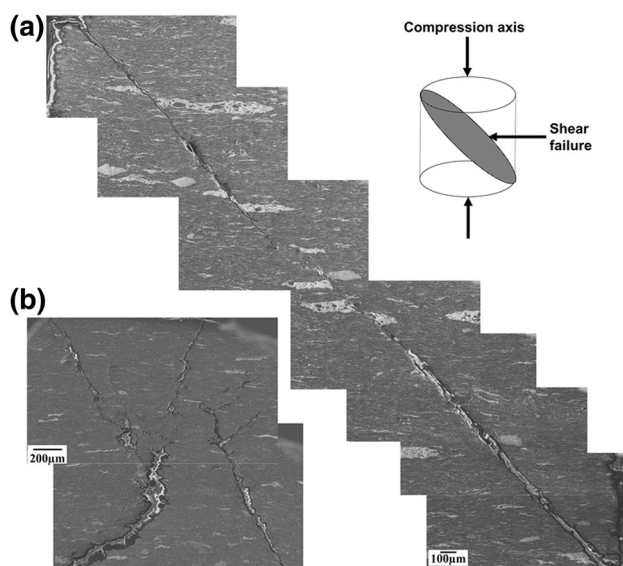


Fig. 12 SEM micrograph of 6061Al compact with **a** 10 and **b** 15 vol.% Pb addition after compression test. Both compacts were prepared through ball-milling and sintered at 590 °C

3.6.2 Quasi-Static Compression Test

Figure 11a shows the engineering stress–strain curve of as-mixed and ball-milled materials subjected to compression test at constant strain rate 10^{-3} s^{-1} . Quasi-static compressive mechanical properties are shown in Fig. 11b. Results indicate that ball-milled materials have higher ultimate compressive and yield strength compared to their counter as-mixed materials. Furthermore, effect of lead volume fraction on ultimate compressive and yield strength shows consistent trend with respect to processing of

material. It is worth noting that these alloys have considerable strain-to-failure ($>15\%$) under quasi-static compression. The maximum yield strength for as-mixed materials are observed at 10 vol.% Pb around 106 MPa. In contrast, ball-milled materials show this value at 5 vol.% Pb around 116 MPa, indicating 9.4% improvement, however, at lower lead content. All samples experience failure around 17–33% engineering strain except ball-milled 6061Al and 6061Al–15Pb alloy which undergoes increased plasticity after yielding. These shows that 0 and 15 vol.% lead added alloy exhibit uniform plastic deformation and indicate good quasi-static compressive ductility as compared to other specimens. The peak ultimate compressive strength and yield strength of the ball milled materials (5 and 10 vol.% Pb), fractured along the maximum shear stress plane, are shown in Fig. 12a. The failure by shear forms at 45° to the direction of applied stress. However, ball-milled 6061Al does not form any crack under quasi-static loading but ball-milled 6061Al–15Pb form crack as shown in Fig. 12b. All as-mixed materials fail at relatively lower strain as compared to the ball-milled material and failure occurs due to cracks in all samples. However, plasticity improves with increase in lead content. The reason for as-mixed material to fail at lower strain can be the presence of micro-voids which acts as crack propagation sites. It should be noted that during compressive deformation in all samples, barreling is observed. To understand the mechanism of failure under quasi-static compression, in-depth analysis is required. Qualitatively, there are number of variables that influence the mechanism of failure under compression that include porosity, microstructure and distribution of second phase particle [41, 42].

4 Conclusions

In this investigation, as-mixed and ball-milled 6061Al–Pb alloys with varying amount of lead content were successfully consolidated through conventional sintering. The effect of lead addition and milling on structural parameter of as-received 6061Al powder was demonstrated. The milling and lead addition significantly enhanced the densification of 6061Al alloys. In case of as-mixed sintered compacts, lead was distributed non-uniformly around the Al matrix. Whereas, ball-milled 6061Al–Pb alloys showed uniform distribution of lead in the microstructure. All sintered compacts exhibited enhancement in hardness with increase in volume fraction of lead and showed nearly 48% increment in hardness due to milling. The ultimate compressive strength of as-sintered 6061Al alloy increased to more than 150% by ball-milling and around 130% by lead addition. The UCS and yield strength for both as-mixed and ball-milled 6061Al alloy were improved with respect to lead volume fraction to a certain limit.

Acknowledgements The authors gratefully acknowledge the characterization facilities and the staff support received from the Advanced Center for Materials Science (ACMS) of Indian Institute of Technology, Kanpur.

Compliance with Ethical Standards

Conflict of interest None.

References

- Hunt W H, *New Directions in Aluminum-Based P/M Materials for Automotive Applications*. SAE Technical Paper (2000).
- Daver E M, Ullrich W J, and Balubhai Patel K, *Key Eng. Mater.*, Trans Tech Publ (1991) 401–428.
- Zhu M, Gao Y, Chung C Y, Che Z X, Luo K C, and Li B L, *Wear* **242** (2000) 47.
- An J, Liu Y B, and Lu Y, *Mater Sci Eng A* **373** (2004) 294.
- Sastry C, and Ranga J G, *Indian J Eng Mater Sci* **17** (2010) 56.
- McAlister A J, *Bull Alloy Phase Diagr* **5** (1984) 69.
- MacKay M L, *Met Prog* **111** (1977) 32.
- Moore K I, Zhang D L, and Cantor B, *Acta Metall Mater* **38** (1990) 1327.
- Mohan S, Agarwala V, and Ray S, *Wear* **157** (1992) 9.
- Benjamin J S, *Metall Trans* **1** (1970) 2943.
- Suryanarayana C, *Prog Mater Sci* **46** (2001) 1.
- Zhu M, Che X Z, Li Z X, Lai J K L, and Qi M, *J Mater Sci* **33** (1998) 5873.
- Apelian D, and Saha D, in Proceedings of Second International P/M Light Alloys Automotive Conference (2000) 1.
- Padmavathi C, and Upadhyaya A, *Trans Indian Inst Met* **64** (2011) 345.
- Ziani A, and Pelletier S, *Int J Powder Metall* **35** (1999) 59.
- Lefebvre L P, and Thomas Y, *Int J Powder Metall* **35** (1999) 45.
- Simchi A, and Veltl G, *Powder Metall* **46** (2003) 159.
- Lumley R N, Sercombe T B, and Schaffer G M, *Metall Mater Trans A* **30** (1999) 457.
- Schaffer G B, Sercombe T B, and Lumley R N, *Mater Chem Phys* **67** (2001) 85.
- Pieczonka T, Schubert T, Baunack S, and Kieback B, *Mater Sci Eng A* **478** (2008) 251.
- Gökçe A, and Findik F, *J Achiev Mater Manuf Eng* **30** (2008) 157.
- Martin J M, Gomez-Acebo T, and Castro F, *Powder Metall* **45** (2002) 173.
- Lumley R N, and Schaffer G B, *Scr Mater* **35** (1996) 589.
- Pathak J P, and Mohan S, *Bull Mater Sci* **26** (2003) 315.
- Sheng H W, Zhou F, Hu Z Q, and Lu K, *J Mater Res* **13** (1998) 308.
- Williamson G K, and Hall W H, *Acta Metall* **1** (1953) 22.
- Suryanarayana C, and Norton M G, *Microsc Microanal* **4** (1998) 513.
- Cullity B D, *Elements of X-Ray Diffraction*. Addison-Wesley, New York, (1978), p 295.
- Prabhu Y T, Rao K V, Kumar V S, and Kumari B S, *World J Nano Sci Eng* **4** (2014) 21.
- Sivasankaran S, Sivaprasad K, Narayanasamy R, and Satyanarayana P V, *Mater Charact* **62** (2011) 661.
- Jeyasimman D, Narayanasamy R, and Ponalagusamy R, *Adv Powder Technol* **26** (2015) 1171.
- Asgharzadeh H, and Simchi A, *Powder Metall* **52** (2009) 28.
- Padmavathi C, Upadhyaya A, and Agrawal D, *Mater Res Innov* **15** (2011) 294.
- Schaffer G B, Hall B J, Bonner S J, Huo S H, and Sercombe T B, *Acta Mater* **54** (2006) 131.
- German R M, *Powder Metallurgy Science*, Met. Powder Ind. Fed., Princeton, NJ (1994), p 290.
- Momeni H, Razavi H, and Shabestari S G, *Iran J Mater Sci Eng* **8** (2011) 10.
- Gaur D K, *Sintering of 6061Al-Alloy and Its Based Composites*, M.Tech Thesis, Indian Institute of Technology, Kanpur, India (1993).
- Youseffi M, and Showaiter N, *Powder Metall* **49** (2006) 240.
- Schaffer G B, and Huo S H, *Powder Metall* **42** (1999) 219.
- Scattergood R O, Koch C C, Murty K L, and Brenner D, *Mater Sci Eng A* **493** (2008) 3.
- Wei Q, Jiao T, Ramesh K T, Ma E, Kecskes L J, Magness L, Dowding R, Kazykhanov V U, and Valiev R Z, *Acta Mater* **54** (2006) 77.
- Liu J, Li S, Fan A, and Sun H, *Mater Sci Eng A* **487** (2008) 235.